Nephrocalcinosis and Nephrolithiasis

Siân Phillips and Gareth R. Tudor

Contents

Abstract

The presence of renal calculi in humans has been identified in mummies discovered as long ago as 4,000 bc, affecting humans for millennia. The underlying aetiology of both nephrocalcinosis and nephrolithiasis is complex. An appreciation of the processes involved in calculus formation aids in the understanding of the diagnosis and management of the disease. The progression of imaging technology has promoted increasingly sensitive and specific techniques in the diagnosis of nephrocalcinosis and nephrolithiasis. Currently, non-contrasted computed tomography has superseded the excretory intravenous urogram in the investigation of acute renal colic because of diagnostic accuracy and ease of application. An understanding of current imaging technology and techniques is necessary to allow its appropriate application in the diagnosis and ongoing management of nephrocalcinosis and nephrolithiasis.

1 Introduction

Nephrolithiasis has been a recognised human disease for millennia. They were found in entombed Egyptian mummies dating back as far as 4,000 BC. The earliest recognised discovery in El Amara was in a teenage boy. Nephrolithiasis is defined as calcification that lies in the collecting system, bladder, ureter and calyceal system. The majority of calculi are found in the pelvicalyceal system and can be passed into the ureter. Nephrocalcinosis is renal calcification that occurs in the renal parenchyma.

With the discovery of modern X-ray by Roentgen, the value of imaging was recognised in the diagnosis and management of nephrolithiasis and nephrocalcinosis. Calcification is easily identified by standard X-rays and computed tomography (CT), the latter bearing the advantage of identification of calculi which is radiolucent on conventional radiographs. This has lead to the increased utilisation of CT in the imaging of nephrolithiasis and nephrocalcinosis. The first paper on intravenous urography was published

S. Phillips (✉) • G.R. Tudor
Department of Radiology, Princess of Wales Hospital, Abertawe Bro Morgannwg University Health Board,
Coity Road, Bridgend CF31 1RQ, Wales, UK
e-mail: sian.phillips5@wales.nhs.uk

E. Quaia (ed.), *Radiological Imaging of the Kidney*, Med Radiol Diagn Imaging,
DOI 10.1007/978-3-642-54047-9_15, © Springer-Verlag Berlin Heidelberg 2014

in 1932, which described the features of a delayed nephrogram and dilated collecting system in a patient with renal colic. This technique was considered to be the most reliable method in the assessment of renal calculi until the advent of helical CT in the early 1990s.

In the UK, acute nephrolithiasis accounts for 1.8/10,000 hospital admissions with an incidence of 7/1,000, with similar figures reported the USA (Sandhu et al. 2003). In the era of increased abdominal cross-sectional imaging, renal calculi are increasingly diagnosed as an incidental finding. The aim of imaging is to identify the presence of nephrocalcinosis and nephrolithiasis and its physiological impact and to plan further management.

2 Nephrocalcinosis

The term nephrocalcinosis describes the deposition of calcium salts in the renal parenchyma. Nephrocalcinosis is a condition, which is a manifestation of different diseases caused by hypercalcaemia and hypercalciuria and can be subdivided into *medullary nephrocalcinosis* or *cortical nephrocalcinosis*. Macroscopic nephrocalcinosis can be classified into two groups: calcification in normal and abnormal tissue. Chemical nephrocalcinosis, relating to the increase of intracellular calcium and microscopic nephrocalcinosis, is not visualised with standard imaging. Metastatic calcification is calcium in normal tissues which is usually due to abnormal biochemistry, i.e. elevated serum calcium. The resultant metabolic imbalance leads to metastatic calcification when the solubility of calcium and phosphate or oxalates in extracellular fluid is exceeded.

Dystrophic calcification is calcium seen in abnormal tissues such as vessels, haematoma, tumours and inflammatory masses and occurs when the solubility of the product of calcium and phosphate is exceeded due to pH changes or a reparative process. This is not considered to be true nephrocalcinosis.

2.1 Causes and Incidence of Nephrocalcinosis

The true incidence of nephrocalcinosis is difficult to establish. Mortensen and Emmett (1954) described the causes of nephrocalcinosis in 91 cases. More recently, Wrong and Feest (1976) described the causes in 375 patients. Cortical nephrocalcinosis accounts for 2.4 % of causes, and medullary nephrocalcinosis accounts for the remaining 97.6 %. The three most common causes of medullary nephrocalcinosis are primary hyperparathyroidism, renal tubular acidosis type 1 and medullary sponge kidney (Figs. 1 and 2).

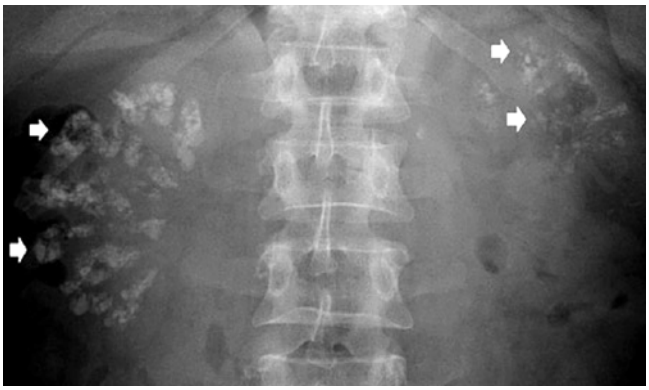

Fig. 1 Plain abdomen radiography demonstrating parenchymal calcifications (*arrows*) in a patient with medullary sponge kidney

Fig. 2 Intravenous excretory urography demonstrating parenchymal calcifications (*arrows*) in a patient with medullary sponge kidney

2.2 Cortical Nephrocalcinosis

Cortical nephrocalcinosis is generally due to severe destructive cortical disease, often seen in patients with end-stage renal failure (Fig. 3). It is seen outlining the periphery of the kidney and along the columns of Bertin.

Cortical nephrocalcinosis may be identified in many pathologic conditions such as acute tubular necrosis, chronic glomerulonephritis, Alport syndrome, prolonged hypercalcaemia and/or hypercalciuria involving many conditions which lead more frequently to nephrolithiasis (hyperparathyroidism,

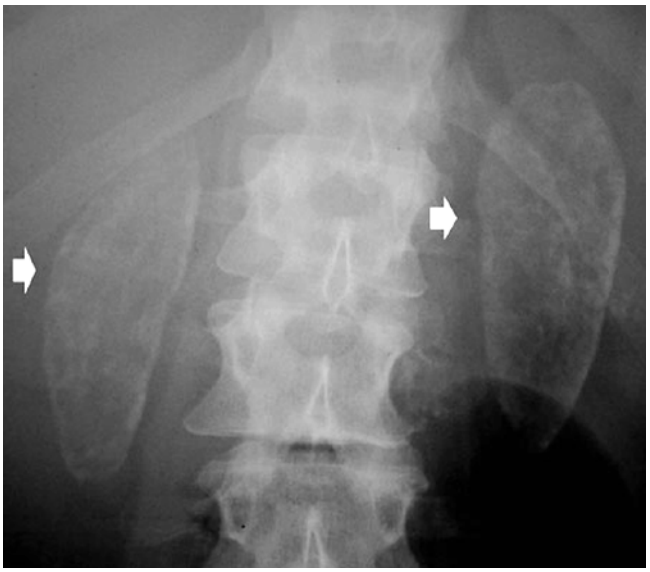

Fig. 3 Plain abdomen radiography demonstrating bilateral uniform cortical nephrocalcinosis (*arrows*)

Fig. 4 Plain radiograph of the pelvis demonstrating cortical calcification (*arrow*) in a transplant kidney

Fig. 5 Plain abdomen radiography demonstrating pyramidal calcification in the right upper pole (*arrows*)

vitamin D intoxication, beryllium poisoning, systemic sarcoidosis, milk-alkali syndrome, hyperthyroidism, Addison disease, idiopathic hypercalcaemia of infancy, increased bone catabolism associated with myeloma, disseminated metastatic bone disease, leukaemia and immobilisation hyperparathyroidism) and chronic renal infections (tuberculosis, AIDS organisms, chronic pyelonephritis) and rejected renal transplants. Ethylene glycol (antifreeze) poisoning can cause marked ballooning and hydropic or vacuolar degeneration of the proximal convoluted tubules and actually corresponds to a form of acute tubular necrosis. Calcium oxalate crystals are usually found in the tubular lumen in such poisonings since ethylene glycol can lead to secondary hyperoxaluria.

Any form of chronic glomerulonephritis can give rise to nephrocalcinosis. The calcification in these cases is seen as fine, granular densities on standard X-rays. Acute cortical necrosis gives rise to patchy calcification, often related to episodes of hypovolaemic shock and eclampsia. Other described causes of cortical nephrocalcinosis include chronic pyelonephritis, Alport syndrome, renal transplants (Fig. 4), oxalosis, polycystic kidney disease and trauma.

2.3 Medullary Nephrocalcinosis

This form of nephrocalcinosis constitutes the most frequently identified type. Medullary nephrocalcinosis is characterised by diffuse calcium deposition within the renal medulla. Underlying causes include medullary sponge kidney, distal renal tubular acidosis, hyperparathyroidism, milk-alkali syndrome, hypervitaminosis D, chronic pyelonephritis, chronic glomerulonephritis, sarcoidosis, glycogen storage disease, Wilson's disease, sickle cell anaemia, infections of the renal medulla, renal papillary necrosis and hyperuricemic (gout, Lesch-Nyhan syndrome) or hypokalaemic conditions (primary hyperaldosteronism, long-term furosemide therapy and Bartter's syndrome). This appears radiologically as small clusters of calcification in the pyramids (Fig. 5). In some causes the pathophysiology is well understood, such as oxalosis and analgesic nephropathy (Figs. 6 and 7). In other cases, the pathophysiology is less well understood, with characteristic association with hypercalcaemia or hypercalciuria. Hyperparathyroidism and renal tubular acidosis are the most commonly recognised causes of medullary nephrocalcinosis along with medullary sponge kidney.

Fig. 6 Intravenous excretory urography in a patient with analgesic nephropathy and a sloughed papilla causing hydronephrosis on the right kidney

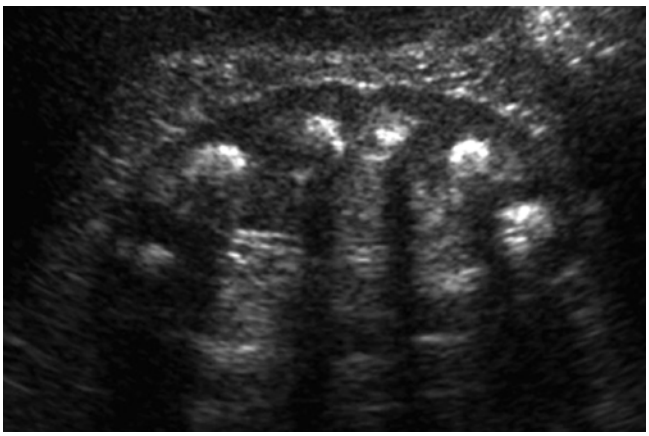

Fig. 8 Ultrasound (*US*) demonstrating extensive medullary calcifications, manifesting with focal hyperechogenicity with posterior acoustic shadowing, in a patient with medullary sponge kidney

Fig. 7 Contrast-enhanced computed tomography (*CT*) demonstrating pyramidal calcifications (*arrow*) in a patient with analgesic nephropathy

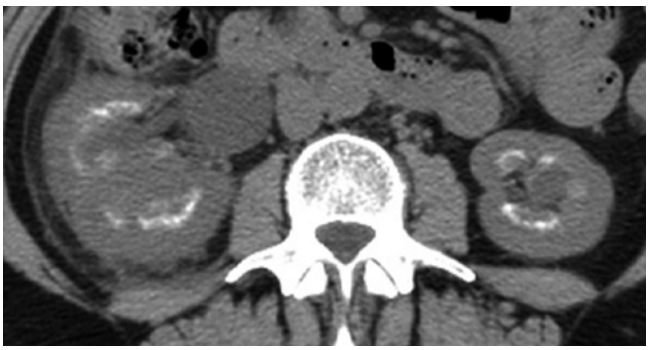

Fig. 9 Unenhanced CT demonstrating extensive parenchymal calcification in a patient with medullary sponge kidney with perinephric stranding and an enlarged kidney

2.3.1 Abnormal Calcium Metabolism

All hypercalcaemic or hypercalciuric states can give rise to medullary nephrocalcinosis. The most common is primary hyperparathyroidism secondary to an adenoma, which causes increased mobilisation of calcium from bone. Hypervitaminosis D, which causes increased absorption of calcium, is a well recognised cause of hypercalcaemia and nephrocalcinosis. This may be accidental, self-induced or iatrogenic. The latter occurs despite normocalcaemia. Other causes include milk-alkali syndrome, sarcoidosis, immobilisation and hyperthyroidism.

2.3.2 Renal Tubular Diseases

Distal renal tubular acidosis is the second most common cause of medullary nephrocalcinosis. Most forms of distal renal tubular acidosis have a high incidence of nephrocalcinosis. The degree of nephrocalcinosis is more severe in these conditions than other causes. Calcium phosphate is believed to be deposited in the collecting ducts after precipitating from the urine. Fanconi's syndrome, Wilson's disease and amphotericin B toxicity are recognised common causes of secondary renal tubular acidosis. Proximal renal tubular acidosis does not manifest itself radiologically.

2.3.3 Medullary Sponge Kidney

The underlying aetiology in medullary sponge kidney is an anatomical defect of cystic dilatation of the distal collecting ducts. There is no underlying metabolic defect. Radiologically, this presents with dense papillary calcification, which has a characteristic appearance (Figs. 8, 9 and 10). The disease may manifest itself unilaterally or segmentally.

3 Nephrolithiasis

Nephrolithiasis is the description of the formation and passing of urinary tract calculi. The terms nephrolithiasis (refers to the kidney) and urolithiasis (refers to the ureter) indicate the presence of calcification(s) within the lumen of the collecting system, ureter and bladder. The commonest clinical manifestation is presentation with acute renal colic. Overall, world prevalence of nephrolithiasis is quoted at 2–3 % (Menon and Resnick 2002); however, this does vary

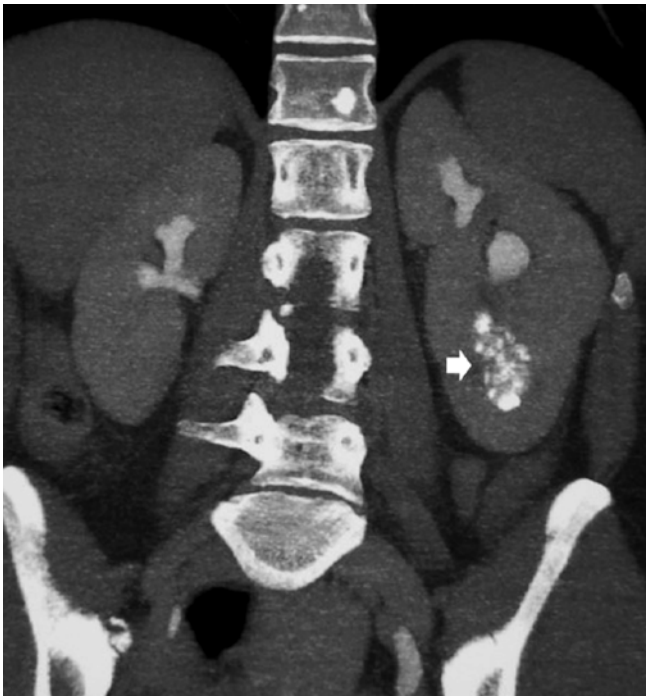

Fig. 10 CT urography. Coronal reformats. Renal sponge kidney with regional medullary nephrocalcinosis (*arrow*) (From the editor E. Quaia)

around the world with different incidences quoted, depending on genetic background, race and climate. Calculus formation is related to an affluent lifestyle in developed countries. Peak incidence occurs in the fourth and fifth decade (Freeman and Sells 2008). Clinically, patients present with acute, severe loin pain when a renal calculus becomes impacted in the ureter causing obstruction, dysuria, strangury, haematuria and recurrent urinary tract infections. They can also present incidentally and chemically with dipstick haematuria, pyuria, sterile pyuria and proteinuria. However, calculi are often asymptomatic, identified as incidental findings on cross-sectional imaging. These incidental findings are, however, important as it can have important lifestyle implications including exclusion from certain occupations such as an airline pilot.

The clinical and metabolic presentation of stone disease can also change over time within various geographical regions. With careful clinical investigation and follow-up, it has been recognised that a cause for calculus formation can be elucidated in 97 % of cases (Rivers et al. 2000). Seventy percent of renal calculi contain calcium, and it is recognised that patients with this form of calculus disease will form further calculi within 7 years (Asplin et al. 1996) (Fig. 11).

The principal locations of renal calculi are calyceal, renal pelvis or ureteropelvic junction. If extracorporeal shock wave lithotripsy (ESWL) is considered, the size, location, and chemical composition of the urinary stones and the assessment of anatomic and functional anomalies in the upper urinary tract are of great importance in order to assess and ensure the smooth passage of the fragmented calculi (Saw et al. 2000; Boll et al. 2009). ESWL is an outpatient procedure, usually administered without anaesthesia. ESWL represents the most common mode of therapy for renal stones, and it is indicated for any type of stones, even though it works better for softer stones such as uric acid stones. A variety of stone characteristics, such as stone size, location and composition, may affect the success of ESWL. ESWL is indicated in the treatment of renal stones <2 cm in diameter.

Ureteric calculi are located distally in the ureter or ureterovesical junction. The American Urological Association published management guidelines for ureteric calculi (Segura et al. 1997). These guidelines recommend that patients whose calculi have a low probability of spontaneous passage (on the basis of their size and location) should be offered intervention. Newer semirigid, fibreoptic ureteroscopes can now be passed with minimal trauma and, in many cases, without dilatation. ESWL remains the first-line treatment for ureteric calculi, regardless of their site, with better results for radiopaque stones less than 1 cm in diameter. For proximal ureteral stones of 1 cm or larger, ESWL, ureteroscopy and percutaneous nephrolithotomy (PCNL) are all acceptable treatments (Teichman 2004). An endoscopic procedure (double J stent) can be inserted prior to ESWL in some cases, such as solitary kidney or large calculi. This decreases the number of complications. ESWL is contraindicated in pregnant patients, bleeding diathesis, uncontrolled hypertension, active urinary tract infections and obstruction distal to the stone. Complications include vascular injury, perirenal haematoma or subcapsular haematoma.

3.1 Incidence and Epidemiology

The risk of developing nephrolithiasis in the adult population varies in different parts of the world. The highest quoted incidence of nephrolithiasis is in Saudi Arabia at 20.1 %, with incidences of 1–5 % in Asia, 5–9 % in Europe and 12–13 % in Canada and North America (Ramello et al. 2000). Nephrolithiasis presents a peak incidence between 20 and 50 years of age and overall male-to-female ratio of 4:1. Epidemiological factors for stone-forming disease include race, sex, age and inherited and individual predisposing factors such as obesity. Environmental factors that influence formation include climate, socio-economic, diet and fluid intake.

3.1.1 Race and Sex

A higher incidence is quoted in males in the Caucasian population, which has been attributed to genetic make-up. However, it is noted that the incidence difference in Black Americans disappears when they adopt a Caucasian diet (Ramello et al. 2000). Conversely, the ratio is quoted as 0.5–0.7, respectively, male-to-female ratios in Black American and Hispanics (Michaels et al. 1994). The higher prevalence of nephrolithiasis in males has been attributed to the effect of

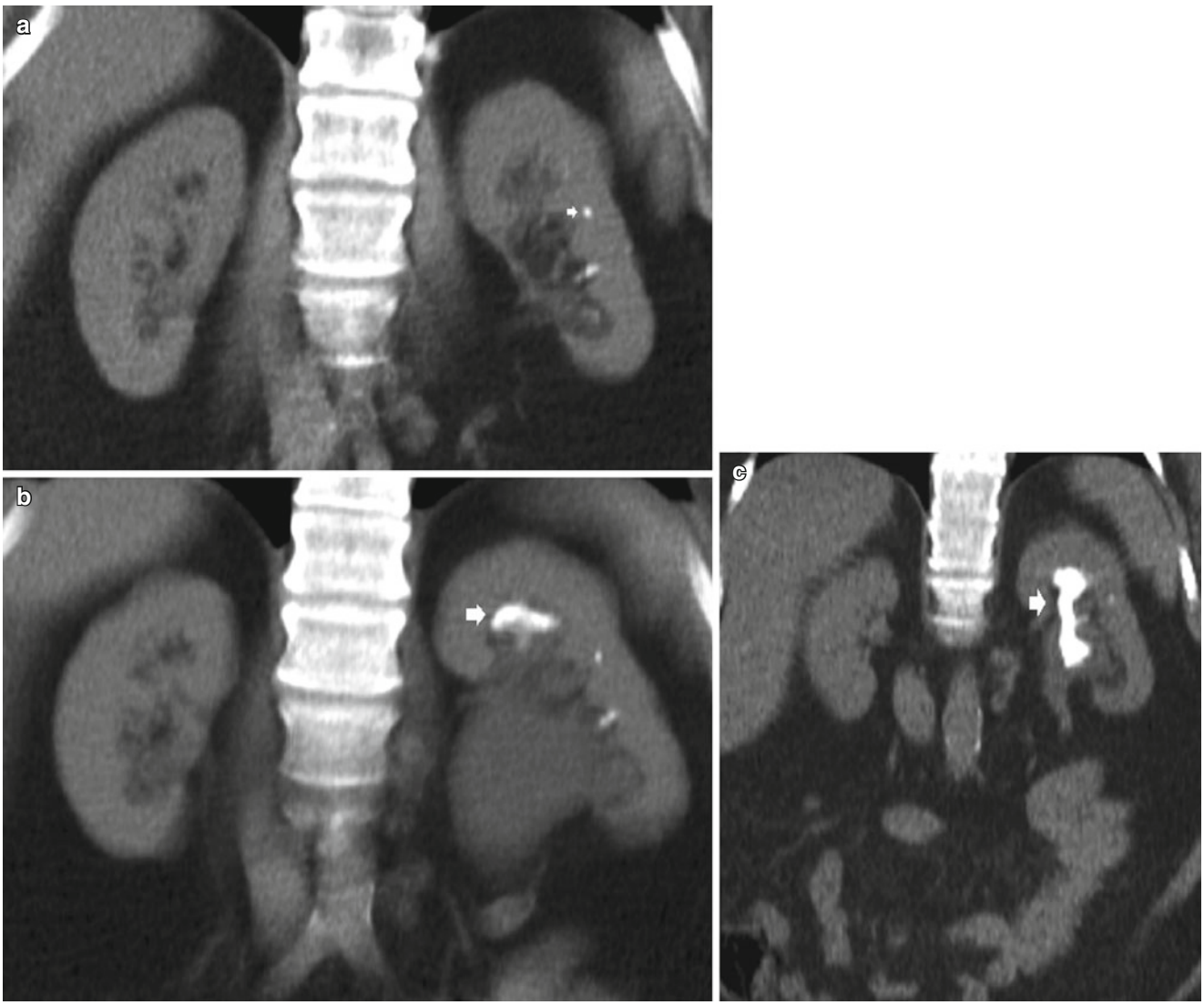

Fig. 11 A series of unenhanced CT coronal acquired over an 18-month period demonstrating initially a calculus (arrow) in the ureter causing hydronephrosis (**a**), then the progressive development of a staghorn calculus (*arrows*) (**b–c**)

androgens (Fan et al. 1999). Recent studies from the USA suggest that there is a changing gender prevalence of stone disease with a change from a 1.7:1 to −1.3:1 male-to-female ratio (Scales et al. 2007). This is speculated to be due to lifestyle factors and obesity.

3.1.2 Age

In idiopathic disease in males, a normal distribution of age is described with a peak incidence at 35 years. Females have a biphasic distribution peak, one at 30 years and the second at 55 years. This is thought to be secondary to calcium reabsorption secondary to the menopause.

3.1.3 Inherited Diseases

The incidence quoted for disease such as cystinuria (autosomal recessive) and hyperoxaluria is scant. Multiple predisposing factors have been identified including general factors (male gender), inherited conditions (polycystic kidney disease, renal tubular acidosis, hyperparathyroidism, cystinuria and hypercalciuria), medications (triamterene, sulphonamides, carbonic anhydrase inhibitors, indinavir, acetazolamide, corticosteroids), low urine volume, hypercalciuria (hyperparathyroidism, sarcoidosis), hyperoxaluria and hypocitraturia (distal renal tubular acidosis). The prevalence of cystinuria is estimated at 2 % in the general population.

3.1.4 Individual Predisposing Factors

Obesity is associated with an increased risk of renal calculi, especially in females with a BMI over 40. Hypertensive patients are more likely to suffer from renal calculus disease. Factors influencing this are complex and may be due to the antihypertensive therapy and other dietary factors.

3.1.5 Environmental Factors

Calculus disease is more prevalent in a temperate climate. This has been described secondary to decreased fluid intake

combined with high plasma vitamin D serum levels secondary to sun exposure.

3.1.6 Socio-economic Factors

Calculus disease is seen as a disease of more affluent nations.

3.1.7 Diet

A high-protein diet has influence on calculus formation risk and calculus composition. Uric acid and calcium oxalate calculi are more prevalent in those with a diet high in animal proteins. The role of dairy products in the pathogenesis of renal calculus disease remains in debate.

3.2 Pathophysiology

Despite significant progress in the treatment of renal calculi, the degree of understanding of the pathogenesis of renal calculus disease has not paralleled this. It has been described that urinary supersaturation is necessary for clinical stone formation. This precipitates crystals to form in the urine. The crystals are believed to be retained in the tubules of the kidney. Several substances found in urine have been demonstrated to precipitate crystal formation, e.g. pyrophosphate, Tamm-Horsfall proteins and magnesium. Noncrystalline organic material, matrix, is then combined with crystal to form calculi. The mode that this occurs remains a source of ongoing research. Several theories have been proposed for pathogenesis. One such theory is crystal-induced renal injury secondary to hyperoxaluria, free particle hypothesis. This proposes that there is a rapid crystal growth in the tubular lumen resulting in crystals being trapped in the papillary collecting duct, resulting in stone formation. An intravascular phenomenon has been proposed with calculi forming as a result of this phenomenon in the vasa recta. Nanobacteria have been proposed as cytotoxic gram-negative bacteria are also implicated in other diseases such as atherosclerosis and periodontal disease. Urinary stasis secondary to anatomic abnormalities is also an identified cause, e.g. hydronephrosis, *ureteropelvic junction obstruction* and horseshoe kidney. Randall's plaques were described over 60 years ago; this suggested that calculi formed around calcium salt deposits in the tip of the renal papilla.

3.3 Types of Calculi

3.3.1 Calcium Calculi

Calcium oxalate stones account for 60 % of all renal stones. This is followed by calcium phosphate types (hydroxyapatite 20 % and brushite 2 %). Hypercalcaemia is the most important pathophysiological risk factor. This can be divided into three categories:

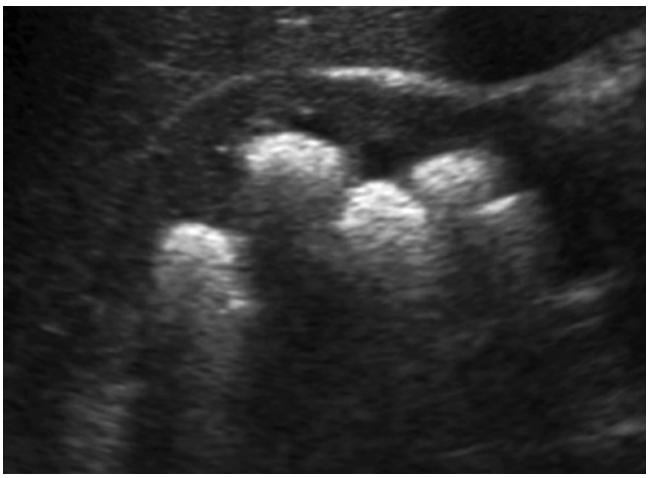

Fig. 12 Greyscale ultrasound. Longitudinal scan. Staghorn renal stone with multiple hyperechogenicities with posterior acoustic shadowing in the renal pelvis

1. Absorptive hypercalciuria due to increased stone absorption of calcium
2. Renal hypercalcaemia due to renal tubular resorption of calcium, which precipitates increasing PTH secretion due to low serum calcium
3. Resorptive hypercalcaemia associated with primary hyperparathyroidism

Other causes of hypercalciuria include malignancy, sarcoidosis, hyperparathyroidism and vitamin D toxicity. Hyperoxaluria, hyperuricosuria and gout can also give rise to calcium oxalate calculi.

Calcium oxalate calculi are dense and therefore relatively well identified on abdominal radiographs.

3.3.2 Cystine Stones

Cystinuria is an autosomal recessive disease that results in a defect in the renal tubular absorption of amino acids, which in turn results in cystinuria. These calculi are only identified on abdominal radiographs if they contain calcium.

3.3.3 Struvite or Infective Calculi

Struvite calculi are composed of magnesium and ammonium phosphate and account for between 7 and 13 % of all renal calculi in the western world (Gleeson and Griffith 1993). They are formed secondary to infection by urease-producing bacteria, most commonly Proteus mirabilis. Struvite does not crystallise in the urine if the pH is less than 7.19. As urinary tract infections are more frequent in women, struvite calculi are seen in females more frequently than males (2:1). Pure struvite calculi are relatively rare; the most common manifestation of struvite calculi is triple stones, calcium-magnesium-ammonium phosphate stones. This is the most common composition of staghorn calculi (Figs. 11, 12 and 13) and is clearly seen on abdominal radiographs. Pure struvite stones are radiolucent.

Fig. 13 CT urography. Coronal reformat. *Staghorn stone in the lower calyceal group of the right kidney*

3.3.4 Uric Acid Calculi

The incidence of uric acid stones varies from 40 % in Israel to 10 % in the USA. They are associated with obesity and type II diabetes. Three factors contributing to uric acid stones are hyperuricosuria, acidic urine and low urinary volume. Low urine pH is often related to medication and also associated with chronic diarrhoea and an ileostomy. A low urinary volume, less than 2 L/day, is considered to predispose to calculus formation. Hyperuricosuria is related to several inherited metabolic disorders such as Lesch-Nyhan syndrome and glycogen storage disease *types I*, *III*, *V and VII*. Uric acid stones are radiolucent on abdominal radiographs. They, however, have sufficient density to be demonstrated in CT and cast an acoustic shadow on ultrasound (US).

3.3.5 Xanthine Calculi

Xanthine calculi are seen in patients with hereditary xanthuria and those undergoing treatment with allopurinol. They are rare calculi with a density similar to that of uric acid calculi and have similar imaging characteristics.

3.3.6 Matrix Calculi

Like struvite calculi, matrix calculi are typically seen in patients with underlying proteus infections, as well as other infections such as *Escherichia coli* and *Candida albicans*. Their composition is mainly of coagulated mucoids with very little calcium component. They are radiolucent on abdominal X-rays.

3.3.7 Indinavir Calculi

Indinavir sulphate is a drug used widely to treat HIV infections. It is a protease inhibitor, and during clinical trials, 4 % of patients receiving the therapy developed calculi. Indinavir crystals are precipitated in the urine forming calculi. These are radiolucent on both plain radiographs and CT (Schwartz et al. 1999). Calcium oxalate and phosphate precipitate within the indinavir crystals, and with time, the density all of the calculi will increase enough to become visible on CT and abdominal radiographs. Contrast-enhanced CT in the delayed phase is valuable in the diagnosis of non-calcified indinavir calculi (Blake et al. 1998).

3.3.8 Oxalate Calculi

Oxaluria may be primary or secondary relating to underlying disorders such as inflammatory bowel disease and short, small bowel syndrome. This occurs due to fat malabsorption leading to saponification of calcium, leaving oxalate unbound, which is then absorbed in the mucosa of the colon.

Patients with coeliac disease as well as Crohn's disease have increased absorption of oxalate from the colon. Patients with inflammatory bowel disease are at increased risk of urolithiasis of all types, with a reported prevalence of 2–12 % (Mcleod and Churchill 1992). Increased consumption of leafy green vegetables that are high in oxalate can also give rise to hyperoxaluria. This results in nephrocalcinosis and progressive formation of calcium oxalate stones. The majority of patients with calcium oxalate stones may not have any detectable abnormality of oxalate metabolite or hyperoxaluria. Oxalate calculi are usually radio-opaque on abdominal radiographs.

4 Imaging

4.1 Background and Principles

The main aims of imaging in patients with acute flank pain that can be related to renal colic are the detection of calculi or the non-stone disease; detection of non-urinary disease related to flank pain; assessment of size, number and location of the stone(s); detection of complications; and evaluation of the contralateral kidney. Four imaging techniques are employed to diagnose renal colic are (1) plain abdominal radiography (kidney-ureter-bladder radiograph; KUB), (2) US, (3) intravenous urography and (4) helical CT.

Identifying the position of calculi anatomically will influence clinical management and intervention. Imaging should establish the physiological impact of the calculus, again influencing the ongoing management of renal disease. Abdominal radiography and intravenous urography were the

Fig. 14 Plain abdomen radiography demonstrating calculi (*arrows*) within calyces of the left kidney

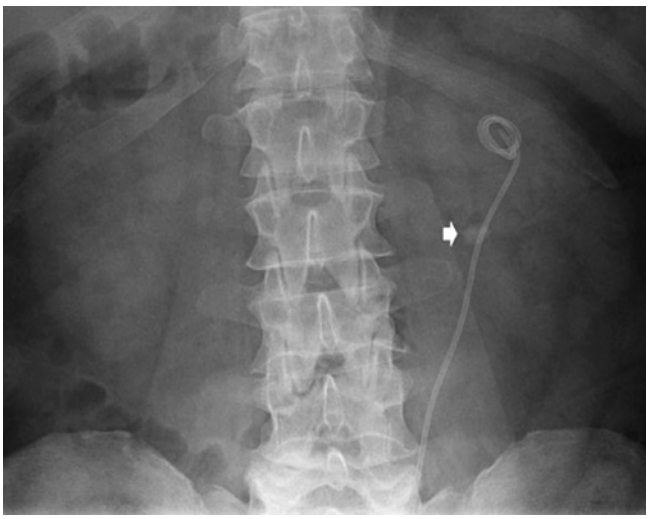

Fig. 15 Plain abdomen radiography with ureteric stent in situ demonstrating a calculus (*arrow*) within the renal pelvis

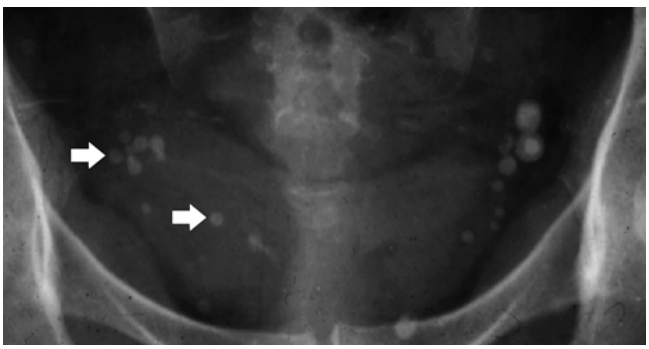

Fig. 16 Plain abdomen radiography. Pelvic phleboliths appearing as multiple round or oval opacities with a central lucency (*arrows*), and lateral to the inferior portion of the sacrum

main stay of imaging strategies until the end of the last century, along with US assessment. The advent of helical CT has seen these modalities largely superseded by a non-contrasted helical CT and excretory CT urography.

4.2 Abdominal Radiographs

The majority (90 %) of renal tract calculi are dense enough to be identified on standard KUB abdominal radiographs (Spirnak et al. 1990) (Figs. 14 and 15). Renal calculi are usually single, polymorphic and with homogeneous opacity. Phleboliths typically appear as multiple round or oval opacities with a central lucency and lateral to the inferior portion of the sacrum (Fig. 16). The sensitivity of the plain abdominal radiography in the detection of urinary calculi ranges from 44 to 77 %, while the specificity ranges from 80 to 87 % (Svedstrom et al. 1990; Haddad et al. 1992; Dalla Palma et al. 2001).

One of the main limitations of this technique is the presence of bowel gas and faecal material within the large bowel, which can obscure small calculi. The principal reasons for the limited visibility of renal stones on the plain radiography are bone overlapping and extra-urinary calcifications including vascular calcifications, calcified lymph nodes, focal zones of compact bone and phleboliths. Patient body habitus can also give rise to interpretation difficulties. In patients presenting with loin pain, the KUB radiograph is often the initial investigation; however, it has been argued that this investigation is not necessary in the investigation of acute renal colic if unenhanced CT is utilised (Kennish et al. 2008).

The KUB is an extremely valuable tool in the follow-up of known renal calculi, especially those undergoing treatment and intervention for calculus disease (Fig. 15).

4.3 Intravenous Excretory Urography

In the USA, this examination has largely been superseded by unenhanced helical CT. However, in Europe and other parts of the world, this technique continues to be utilised where access to CT scanning may be limited. Intravenous excretory urography is a time-consuming technique, especially in obstructed patients; adds the risks of iodinated contrast administration; and is not suggested in acute ureteral obstruction due to contrast-induced diuresis.

The technique involves the intravenous administration of low-osmolality nonionic contrast medium and examination of the renal tract with targeted abdominal X-rays at selected

Fig. 17 Intravenous excretory urography demonstrating a right staghorn calculus (*arrow*) appearing as a complex filling defect in the dilated renal pelvis

Fig. 18 Digital tomosynthesis IVU demonstrating renal calculi (*arrows*) within the lower pole calyces of the left kidney

time intervals. This will identify the position and anatomical location of calculi, along with a degree of obstruction if the calculus has passed into the ureter (Fig. 17).

The reported sensitivity of this technique for identifying calculi is 84–95 %, but this falls when small calculi are considered (Miller and Kane 2000). The main disadvantage of this technique is the possible patient adverse reaction to intravenous contrast media, although this is small with non-ionic contrast media. Also, precise anatomical delineation is suboptimal if interventional techniques are considered. In this case, a CT should be performed for superior anatomical reference. The examination is contraindicated in patients with renal impairment and a serum creatinine over 150 mmol/L. It is recognised that some calculi are not identified with this technique with a detection rate of 69 % (Dalla Palma et al. 2001). The utilisation of linear tomography has largely disappeared.

Digital tomography is a new technique that demonstrates promise, but this has yet to be fully evaluated in the context of other imaging modalities in the evaluation of the renal tract (Fig. 18). The findings of renal tract obstruction on intravenous urography include absent nephrogram, delayed nephrogram, renal enlargement, delayed pyelogram, extravasation of contrast, hydronephrosis, asymmetry in contrast density and delayed emptying of the collecting system.

4.4 Ultrasound

US can be employed to detect hydronephrosis, to identify calculi, to assess the renal size and renal parenchyma thickness and to detect complications. In non-hydrated patients, US presents a sensitivity of 24–73 % (Fowler et al. 2002) and a specificity of 74 %, while the sensitivity becomes 85–100 % and the specificity 83–100 % in hydrated patients (Middleton et al. 1988; Svedstrom et al. 1990; Haddad et al. 1992; Dalla Palma et al. 1993). *US has a low sensitivity (20–30 %) and high specificity (90 %) in the detection of renal stones, while it presents a moderate sensitivity (60–70 %) and high*

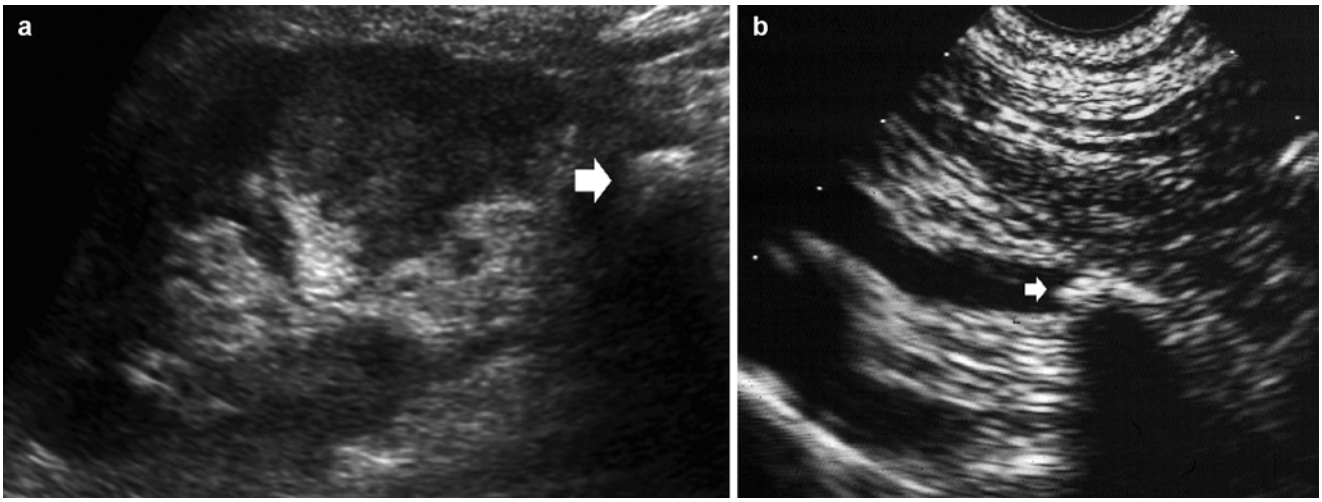

Fig. 19 (**a**) Greyscale ultrasound. Longitudinal scan. A calculus (*arrow*) with posterior acoustic shadowing is visualised in the lower pole of the left kidney. (**b**) Greyscale ultrasound. Longitudinal scan. A calculus (*arrow*) with posterior acoustic shadowing is visualised in the distal ureter

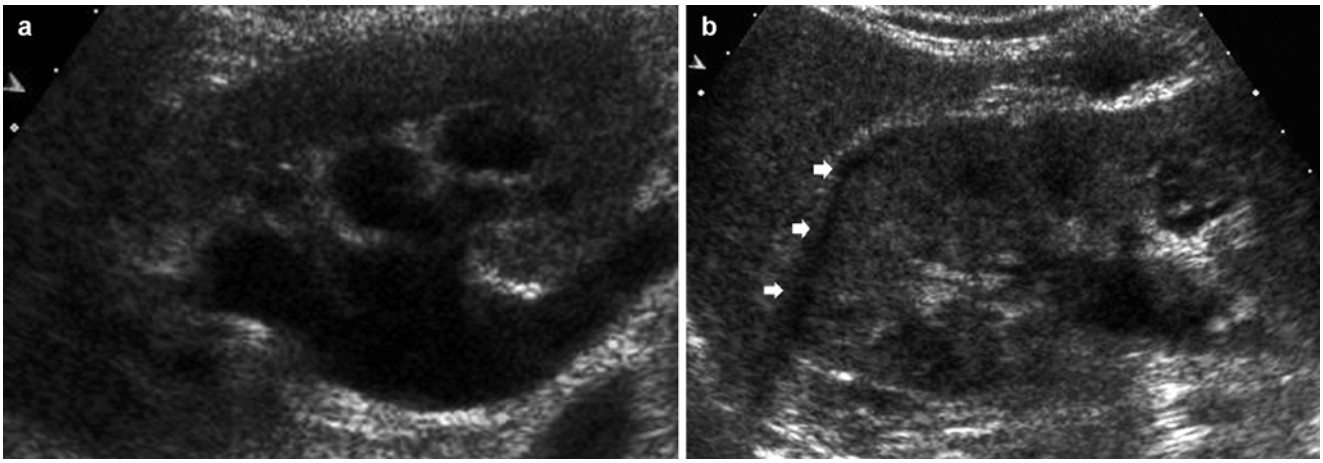

Fig. 20 Greyscale ultrasound. Indirect signs of renal colic. (**a**) Dilatation of the intrarenal urinary tract; (**b**) subcapsular collections corresponding to urinoma (*arrows*) (Courtesy of Prof. E. Quaia)

specificity (*90–95 %*) (Fowler et al. 2002) *in the detection of ureteral stones*. The main variables affecting the US sensitivity in detecting urinary stone are the calculus size and position, and patient body habitus, while calculus composition does not affect the diagnostic sensitivity and specificity of US. US allows the evaluation of the kidney and pelvis provided that the bladder is distended.

Renal and ureteral calculi are characteristically identified on US as echogenic foci with an acoustic shadow (Fig. 19). Renal calculi need to be 5 mm to be identified consistently on US, and US can identify calculi that are radiolucent on KUB X-ray. The detection of urinary stones and clarity of posterior shadowing are significantly improved by harmonic imaging (Ozdemir et al. 2008). The other US findings in a patient with renal colic, besides the direct identification of the calculus, consist of increased echogenicity of renal parenchyma, pelvicalyceal and ureteric dilatation and subcapsular collections (urinomas) (Fig. 20).

Doppler US techniques are utilised to demonstrate haemodynamic changes that occur with obstruction, which result in intrarenal vascular resistance with associated rise in the resistance resistive index (RI). Duplex Doppler sonography has been reported to be a useful non-invasive imaging method for the diagnosis of renal obstruction. A mean RI >0.7, a difference >0.08–0.1 between the mean RI of the two kidneys and a progressive increase in RI following fluid administration and diuretics have been considered diagnostic of obstruction (Platt 1992; Platt et al. 1993). The evaluation of renal parenchyma RIs presents a controversial role in the acute renal colic with a sensitivity from 19 to 92 % and a specificity from 88 to 98 % according to the different series (Platt et al. 1989a, b; Tublin et al. 1994; Platt 1996).

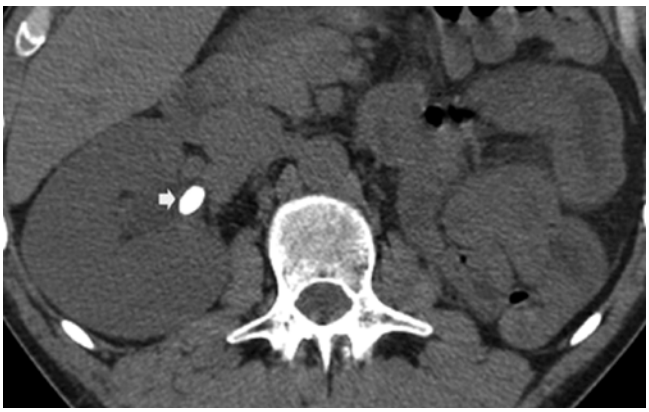

Fig. 21 Unenhanced CT scan demonstrating a right renal pelvis calculus (*arrow*) in a patient with solitary kidney

This is determined by the absence of a true reference standard to diagnose renal obstruction and by the possible presence of partial and intermittent obstruction.

It has been suggested that colour Doppler US along with KUB X-ray could be adopted the initial investigation of renal colic; however, this has not been adopted in general clinical practice (Haddad et al. 1994). Twinkle artefact – also named colour comet-tail artefact (Campbell et al. 2004; Tchelepi and Ralls 2009) or sparkle sign – facilitates the detection of calculi, providing information on their chemical composition. It is determined by the random Doppler shift in the shadow of the stone and depends on the roughness of the surface of the stone. It is not visible in calcium oxalate calculi. Twinkle artefact may also be helpful in identifying calculi that are poorly echoic and lacking discrete shadowing (Fig. 21).

The detection of ureteral jets by colour Doppler does not imply the absence of obstruction, since ureteral jets may be identified also in partial ureteral obstruction (Burge et al. 1991; Cox et al. 1992). The visibility of the ureteral jets depends on the flow velocity and density gradient between the urine in the bladder and ureter. This represents a time-consuming assessment and is not routinely employed.

The role of US in the follow-up of renal calculi is limited, with KUB and CT being more informative (Fowler et al. 2002). US is the preferred imaging modality in pregnancy over excretory urography, with incidence of renal stones equal to that in the non-pregnant female. This technique enables visualisation of the kidney and identification of calculi and obstruction without utilisation of ionising radiation. Filling defects on intravenous urography can be identified as being either soft tissue (e.g. clot or tumour) or renal calculi, on the basis of US. The role of US in the follow-up of renal calculi, which is being conservatively managed or undergoing treatment with extracorporeal shockwave lithotripsy (ESWL), is limited. It is difficult to reproduce measurements consistently with poorer spatial resolution and the associated issues surrounding a user-dependent technique.

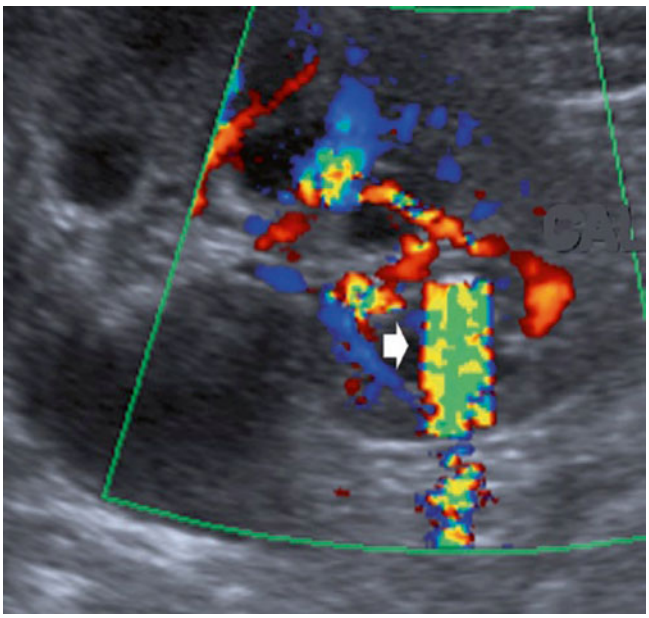

Fig. 22 Ultrasound image demonstrating the sparkle sign or twinkle artefact sign (*arrow*) due to a calculus in a lower pole calyx (Courtesy of Dr F Bowyer)

Fig. 23 Coronal CT reformations showing lower pole calculi (*arrow*) in the left kidney

4.5 Computed Tomography

The advent of multidetector row helical CT has revolutionised the imaging of renal calculi and nephrocalcinosis. Multidetector row CT allows image acquisition in a single breath hold with thin collimation (Figs. 22 and 23). With ever-improving technology, this has allowed improvement in spatial, temporal and contrast resolution; the images obtained

are of ever-increasing quality. The ability to perform multiplanar reformats (MPR) in orthogonal, oblique and curved planes, along with volume rendering and reconstruction techniques, optimises the anatomical delineation of the study. Accurate determination of the stone burden is a major advantage of this technique over IVU and linear tomography. The ability of CT to diagnose non-opaque calculi was recognised as far back as the 1970s (Segal et al. 1978). Ninety-nine percent of calculi can be identified on CT, even though they are radiolucent on standard radiographs. Indinavir and pure matrix calculi are sometimes not identified on CT. There are two main techniques described for imaging of the renal tract by CT, non-contrasted helical CT and excretory CT urography.

4.5.1 Unenhanced CT

This technique was developed in the mid-1990s (Smith et al. 1995). It is currently the mainstay in the evaluation of renal calculi, especially in the USA and large parts of Europe, where some departments have completely abandoned intravenous urography in favour of CT techniques (Amis 1999; Silverman et al. 2009). This simple technique does not involve any patient preparation, oral or intravenous contrast with minimal imaging time. There is an increased radiation dose compared with intravenous urography; hence low-dose techniques are advocated (Tack et al. 2003; Hamm et al. 2002; Nawfel et al. 2004) (Figs. 24 and 25).

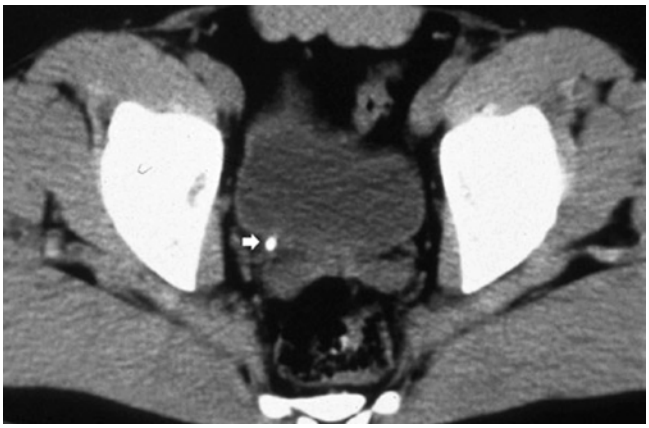

Fig. 24 Unenhanced CT image demonstrating a ureteral stone (*arrow*) in the distal right ureter

An optimally protocoled CT examination with low exposure factors does maintain its diagnostic accuracy (Meagher et al. 2001; Memarsadeghi et al. 2005). Unenhanced CT is more effective than intravenous urography in precisely identifying ureteric stones and is equally effective as IVU in the determination of the presence or absence of ureteric obstruction (Smith et al. 1995). Nowadays, thin-section 1-mm collimation with a low pitch is possible in multidetector CT imaging of the urinary tract. Examinations are usually performed by using 120 kVp tube voltage; 16 (detector rows) × 0.75-mm (section thickness), 64 × 0.5-mm or 32 × 1-mm collimation; and 2-mm interval reconstruction. The tube current (100–330 mA, with a mean of 150 mA) is adjusted for each examination, according to patient body habitus, by using automated dose modulation algorithm.

The technique has a high sensitivity (94–100 %) and specificity (93–98 %) (Dalla Palma et al. 2001) with the added benefit of being able to identify alternative pathologies, which can mimic renal colic, such as pyelonephritis, hepatobiliary disease and vascular conditions (Rucker et al. 2004). Although this technique is more expensive than US and IVUs, it is considered to be more cost effective (Pfister et al. 2003). Patients are scanned in the supine position in a single breath hold. Prone scanning is advocated to demonstrate renal calculi that have passed to the vesicoureteric

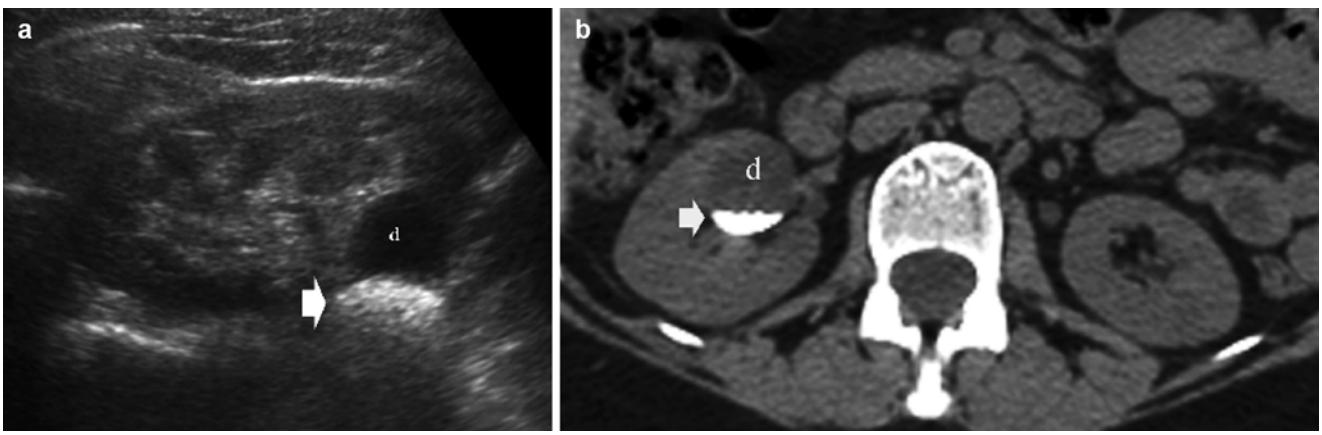

Fig. 25 (**a**) Ultrasound of the right kidney demonstrating echogenic stone (*arrow*) within a calyceal diverticulum indicated by the letter *d*. (**b**) Unenhanced CT demonstrating the renal stone (*arrow*) within a calyceal diverticulum indicated by the letter *d*

junction VUJ (Levine et al. 1999). The ability to reconstruct images in coronal and sagittal planes is beneficial. Reformatted images can then be performed in the coronal plane. Clinicians often prefer coronal reformatted images to review the data as it replicates the visual presentation of an intravenous urogram.

Unenhanced CT shows direct and indirect findings of colic pain due to stone. The direct finding is the visualisation of the calculus itself (Figs. 22, 23, 24 and 25). Regardless of composition, almost all renal stones are detected at unenhanced CT because the attenuation of stones is higher than that of surrounding tissue, even though the attenuation of uric stones is lower than the attenuation of calcium stones (Taourel et al. 2008). Indirect signs include ureteral dilatation (frequency: 65–90 %) (Fig. 26a) with or without perirenal urinoma (Fig. 26b), perinephric (Fig. 27) and periureteral (Fig. 28) stranding (36–82 %), renal enlargement (frequency 36–71 %) and reduced attenuation (>5 HU) of the renal parenchyma (pale kidney sign) (Georgiades et al. 2001; Goldman et al. 2004), renal sinus fat blurring (Fig. 29) (Smith et al. 1996; Niall et al. 1999; Sourtzis et al. 1999) and the rim sign around the ureter (frequency 50–77 %) (Fig. 30).

An early sign of acute ureteric obstruction is the effacement of pelvicalyceal fat, perinephric oedema or stranding in the perinephric space and may evolve into a frank perinephric fluid collection. Boridy et al. (1999) described this as *being due to urine infiltrating into the perinephric space* along the bridging septa of Kuhn, possibly a result of pyelolymphatic backflow (Fig. 27). Differential diagnoses that should always be considered in patients presenting with perinephric stranding on CT are pyelonephritis, renal vein thrombosis and renal infarction.

The most important challenge in the interpretation of unenhanced CT in the evaluation of patients with suspected urolithiasis is the frequent inability to identify the ureter among periureteral vessels and to differentiate urinary calculi from extra-urinary calcifications, in particular from phleboliths. The rim sign is specific for the urinary stone, while the comet-tail sign is specific for phleboliths (Fig. 31). The comet-tail sign consists in the eccentric tapering of soft tissue extending from one surface of the calcification. Moreover, most phleboliths are round or oval, while most renal or ureteral calculi are slightly angular in shape. Phleboliths may contain a central lucent area, even though this is rarely observed on CT (Traubici et al. 1999).

Another important task of unenhanced CT is the differentiation of renal colic from other causes of acute flank pain including diverticulitis or appendicitis, pelvic masses, large renal tumours, bowel obstruction and aortic aneurysm. Most of these pathologic entities are identified on unenhanced CT. The advantage of unenhanced CT to evaluate for renal calculi in the acute setting is the identification of extrarenal

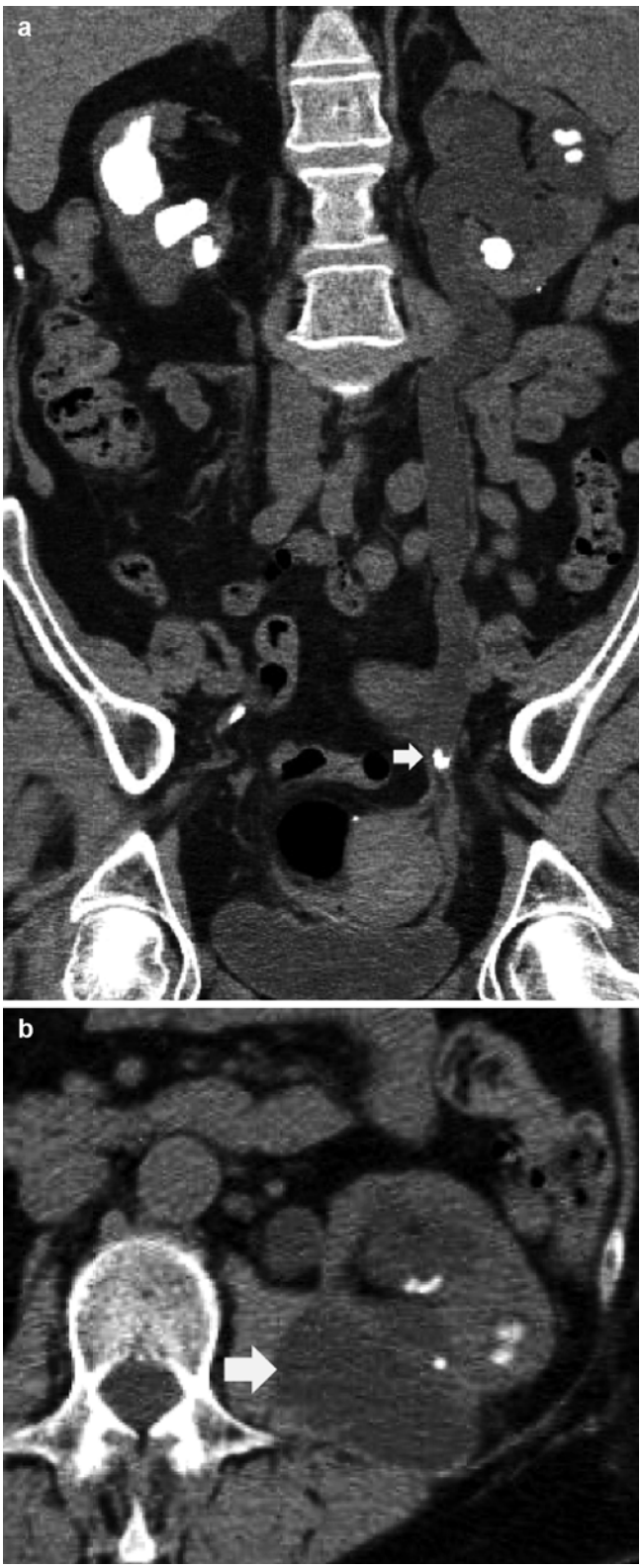

Fig. 26 Indirect signs of renal calculi. (**a**) Unenhanced CT. Coronal reformation. Left urinary tract dilatation due to an obstructing ureteral stone (*arrow*). Multiple renal calculi are evident on the left kidney, while staghorn calculosis is depicted on the right kidney. **b** Unenhanced CT. Transverse plane. Perirenal urinoma (*arrow*) (Courtesy of Prof. E. Quaia)

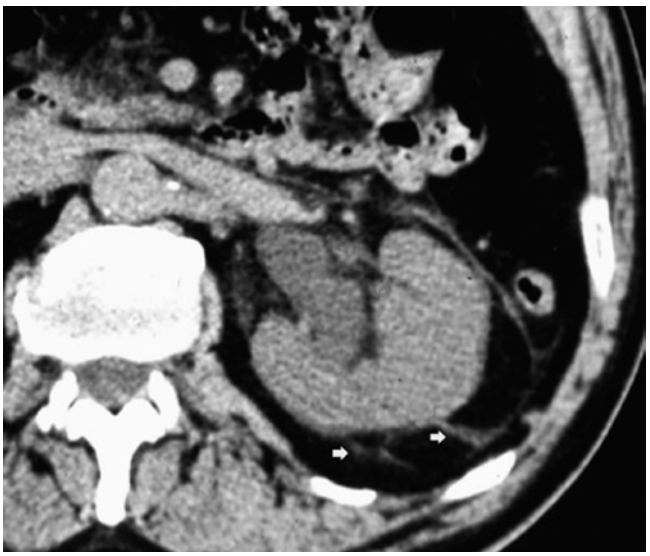

Fig. 27 Indirect signs of renal calculi. Unenhanced CT. Transverse plane. Perinephric strandings (*arrows*) surrounding the enlarged left kidney with dilatation of the intrarenal urinary tract (Courtesy of Prof. E. Quaia)

Fig. 29 Indirect signs of renal calculi. Unenhanced CT. Transverse plane. Renal sinus fat blurring (*arrow*) with increased density of the sinus fat (Courtesy of Prof. E. Quaia)

Fig. 28 Indirect signs of renal calculi. Unenhanced CT. Transverse plane. Periureteral strandings (*arrow*) with dilatation of the distal ureter presenting a stone (Courtesy of Prof. E. Quaia)

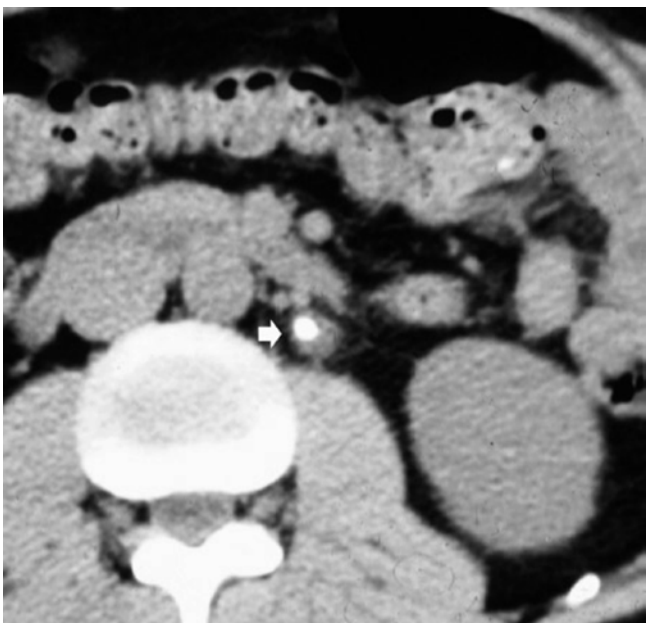

Fig. 30 Indirect signs of renal calculi. Unenhanced CT. Transverse plane. Rim sign (*arrow*) around the dilated ureter with a renal *calculus* (Courtesy of Prof. E. Quaia)

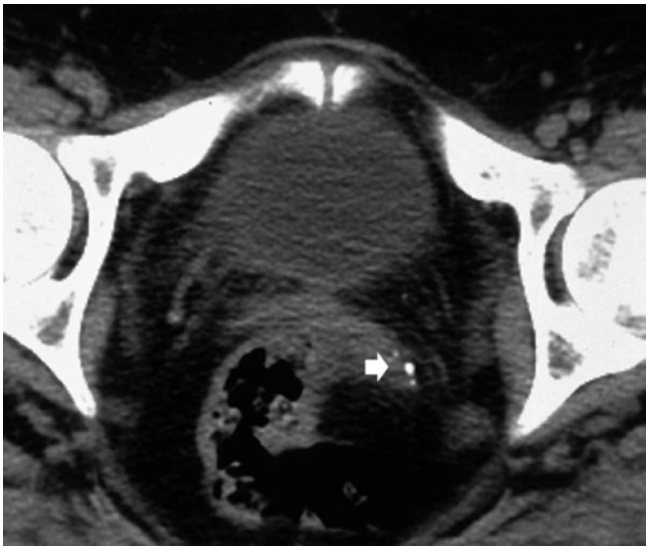

Fig. 31 Indirect signs of renal calculi. Unenhanced CT. Transverse plane. Comet-tail (*arrow*) adjacent to pelvic phleboliths consisting of eccentric tapering of soft tissue extending from one surface of the calcification (Courtesy of Prof. E. Quaia)

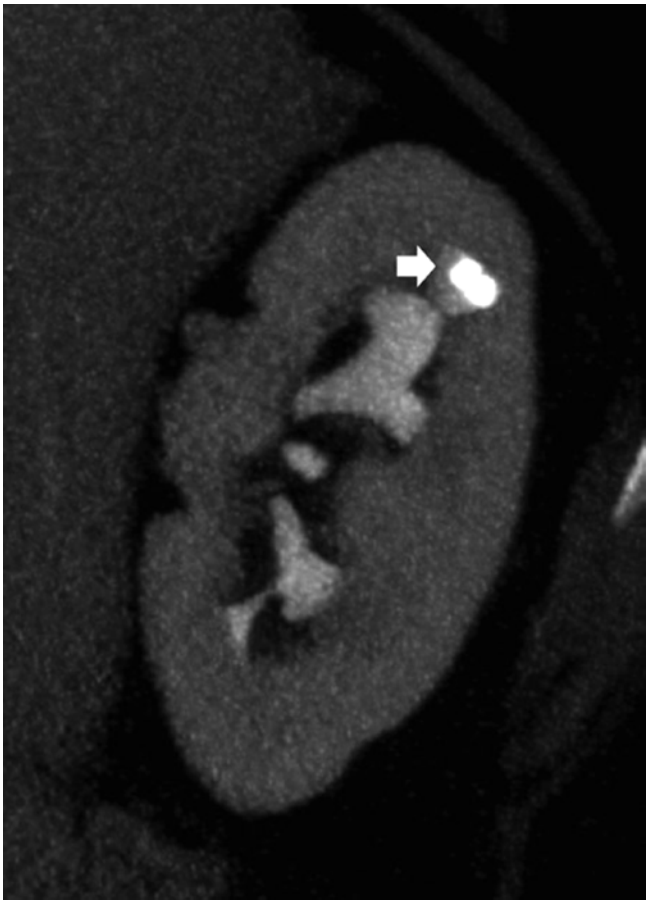

Fig. 32 CT urography. Coronal reformation. Renal calculus within a calyceal diverticulum (*arrow*) on the upper calyces of the left kidney (Courtesy of Prof. E. Quaia)

diagnoses such as appendicitis, gynaecological disease and, most notably, ruptured abdominal aortic aneurysms whose clinical presentation can frequently mimic renal colic.

Site, size and density of renal calculi can be determined by CT, a density of greater than 1,000 HU being considered to be less responsive to ESWL (Joseph et al. 2002). Theoretically, CT also has the ability to identify the chemical composition of renal calculi; this, however, has not been adopted into clinical practice (Hillman et al. 1984; Deveci et al. 2004). The dual-energy CT attenuation value can be used to predict the chemical composition of the stones in vitro (Grosjean et al. 2008; Thomas et al. 2009; Boll et al. 2009). This ability indicates the strength of CT as an imaging tool over that of intravenous urography or US. The identification of cystine and calcium oxalate would be beneficial as they are relatively resistant to ESWL. Nakada et al. (2000) described the ability to differentiate between uric acid and calcium oxalate stones in the clinical setting. Three-dimensional (3D) reconstructions can add greater anatomical information. Which is beneficial when intervention is considered may influence the choice of ESWL and PCNL.

Since the radiation exposure from KUB is 0.5–0.9 mSv, from intravenous urography is 1.33–3.5 mSv, while from regular dose CT is 4.3–16.1 mSv, the employment of low-dose unenhanced CT is advocated. In single-slice CT, the higher the pitch, the lower the corresponding dose; however, in multidetector CT, the lower the current tube (mA), the lower the corresponding dose (Mahesh et al. 2001). With the most recent low-dose CT protocols, it is possible to achieve a dose of 0.97–1.35 mSv (Knopfle et al. 2003), while with ultra-low-dose CT (20 mA), a dose of 0.5–0.7 mSv (Kluner et al. 2006).

4.5.2 CT Urography

This technique is the CT examination of renal imaging tract after the administration of intravenous contrast, with delayed imaging to visualise the collecting systems and lower tracts during the excretory phase.

CT urography is being introduced for 3D evaluation of those patients with complex renal calculus disease in whom PCNL is considered (Patel et al. 2009). This technique allows optimal anatomical delineation both for renal (Fig. 32) and urinary stones (Figs. 33 and 34). The most common indication for this procedure is the investigation of microscopic haematuria in the examination of the urothelium for upper and lower tract neoplastic lesions (Silverman et al. 2009).

Fig. 33 CT urography. Coronal reformation. Mild hydronephrosis on the left kidney with an obstructing calculus in the proximal ureter (*arrow*). Right pelvicalyceal drainage is normal with IV contrast seen in the right ureter (Courtesy of Prof. E. Quaia)

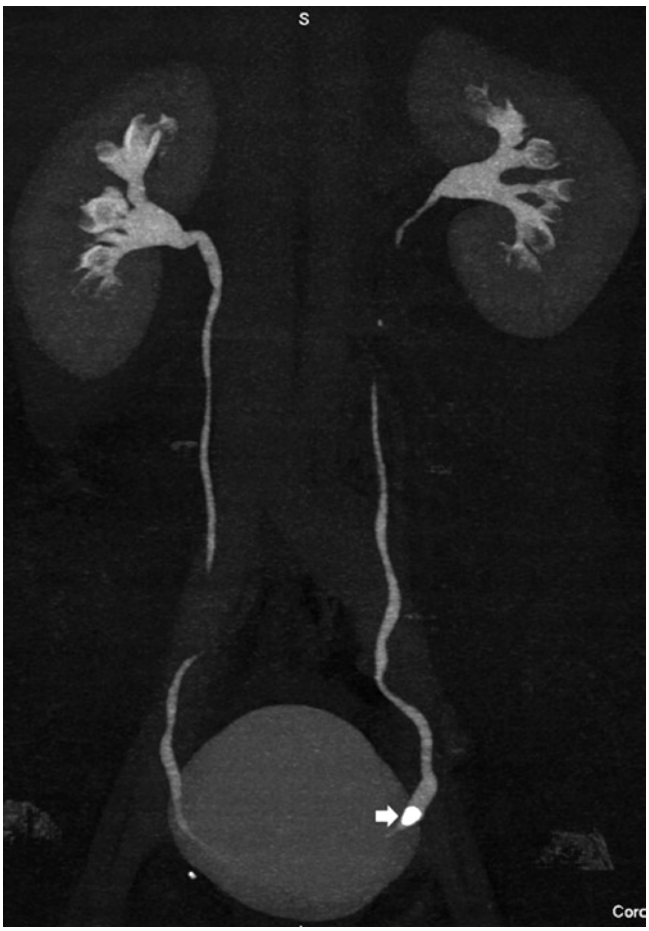

Fig. 34 CT urography. Maximum intensity projection. A calculus is visualised in the distal ureter (*arrow*) (Courtesy of Prof. E. Quaia)

The technique utilised varies widely from department to department; optimal protocols have yet to be decided (Townsend et al. 2009). There are reports of dual-energy contrast-enhanced CT, relating to the ability of this technique to subtract the contrast-enhanced data set, creating virtual unenhanced CT images (Scheffel et al. 2007).

4.6 Other Techniques

Magnetic resonance urography (MRU) has been universally adopted as a non-ionising radiation investigation of the renal tract. The technique has a limited role in the evaluation of renal calculi, although has demonstrated benefit on examination of the renal tract in specific groups such as those of pregnant patients presenting with symptoms of ureteric colic. It can be useful to differentiate between physiological hydronephrosis and ureteric calculi. This technique enables reconstruction of the images from the raw data set to present images that mimic a conventional IVU. Spatial resolution is, however, poor. There may also be difficulty in differentiating filling defects seen on MRU, the appearances of early urothelial tumours and small calculi being very similar (Girish et al. 2004).

References

Amis ES Jr (1999) Epitaph for the urogram. Radiology 213:639–640

Asplin JR, Favus MJ, Coe FL (1996) Nephrolithiasis. In: Brenner BM (ed) The kidney. WB Saunders, Philadelphia, pp 1893–1935

Blake SP, McNicholas MM, Raptopoulos V (1998) Non opaque crystal deposition causing ureteric obstruction in patients with HIV undergoing indinavir therapy. AJR Am J Roentgenol 171:717–720

Boll DT, Patil NA, Paulson EK et al (2009) Renal stone assessment with dual-energy multidetector CT and advanced postprocessing techniques: improved characterization of renal stone composition – pilot study. Radiology 250:813–820

Boridy IC, Kawashima A, Goldman SM et al (1999) Acute ureterolithiasis: nonenhanced helical CT findings of perinephric oedema for prediction of degree of ureteral obstruction. Radiology 213:663–667

Burge HJ, Middleton WD, McClennan BL et al (1991) Ureteral jets in healthy subjects and in patients with unilateral ureteral calculi: comparison with color Doppler US. Radiology 180(2):437–442

Campbell SC, Cullinnan JA, Rubens DJ (2004) Slow flow or no flow? Color and power Doppler US pitfalls in the abdomen and pelvis. Radiographics 28:497–506

Cox IH, Erickson SJ, Foley WD et al (1992) Ureteric jets: evaluation of normal flow dynamics with color Doppler sonography. AJR Am J Roentgenol 158:1051–1055

Dalla Palma L, Stacul F, Bazzocchi M et al (1993) Ultrasonography and plain film versus intravenous urography in ureteric colic. Clin Radiol 47(5):333–336

Dalla Palma L, Pozzi-Mucelli R, Stacul F (2001) Present-day imaging of patients with renal colic. Eur Radiol 11:4–17

Deveci S, Co kun M, Tekin M et al (2004) Spiral computed tomography: role in determination of chemical compositions of pure and mixed urinary stones-an in vitro study. Urology 64:237–240

Fan J, Chandhoke PS, Grampas SA (1999) Role of sex hormones in experimental calcium oxalate nephrolithiasis. J Am Soc Nephrol 10:S376–S380

Fowler KA, Locken JA, Duchesne JH et al (2002) US for detecting renal calculi with nonenhanced CT as a reference standard. Radiology 222:109–113

Freeman SJ, Sells S (2008) Investigation of loin pain. Imaging 20:38–56

Georgiades CS, Moore CJ, Smith DP (2001) Differences of renal parenchymal attenuation for acutely obstructed and unobstructed kidneys on unenhanced helical CT: a useful secondary sign? AJR Am J Roentgenol 175:325–330

Girish G, Chooi WK, Morocos SK (2004) Filling defect artefacts in magnetic resonance urography. Eur Radiol 14:145–150

Gleeson MJ, Griffith DP (1993) Struvite calculi. Br J Urol 71:503–511

Goldman SM, Faintuch S, Ajzen SA et al (2004) Diagnostic value of attenuation measurements of the kidney on unenhanced helical CT of obstructive ureterolithiasis. AJR Am J Roentgenol 182:1251–1254

Grosjean R, Sauer B, Guerra RM et al (2008) Characterization of human renal stones with MDCT: advantage of dual energy and limitations due to respiratory motion. AJR Am J Roentgenol 190:720–728

Haddad MC, Sharif HS, Shahed MS et al (1992) Renal colic: diagnosis and outcome. Radiology 184:83–88

Haddad MC, Sharif HS, Abomelha MA et al (1994) Colour Doppler sonography and plain abdominal radiography in the management of patients with renal colic. Eur Radiol 4:529–532

Hamm M, Knopfle E, Wartenberg S et al (2002) Low dose unenhanced helical computerized tomography for the evaluation of acute flank pain. J Urol 167:1687–1691

Hillman BJ, Drach GW, Tracey P et al (1984) Computed tomographic analysis of renal calculi. AJR Am J Roentgenol 142:549–552

Joseph P, Mandal AK, Singh KL et al (2002) Computerized tomography attenuation value of renal calculus: can it predict successful fragmentation of the calculus by extracorporeal shock wave lithotripsy? A preliminary study. J Urol 167:1968–1971

Kennish SJ, Bhatnagar P, Wah TM et al (2008) Is the KUB radiograph redundant for investigating acute ureteric colic in the non-contrast enhanced computed tomography era? Clin Radiol 63:1131–1135

Kluner C, Hein PA, Gralla O et al (2006) Does ultra-low-dose CT with a radiation dose equivalent to that of KUB suffice to detect renal and ureteral calculi? J Comput Assist Tomogr 30(1):44–50

Knöpfle E, Hamm M, Wartenberg S et al (2003) CT in ureterolithiasis with a radiation dose equal to intravenous urography: results in 209 patients. Röfo 175(12):1667–1672

Levine J, Neitlich J, Smith RC (1999) The value of prone scanning to distinguish ureterovesical junction stones from ureteral stones that have passed into the bladder: leave no stone unturned. AJR Am J Roentgenol 172:977–981

Mahesh M, Scatarige JC, Cooper J et al (2001) Dose and pitch relationship for a particular multislice CT scanner. AJR Am J Roentgenol 177(6):1273–1275

McLeod RD, Churchill DN (1992) Urolithiasis complicating inflammatory bowel disease. J Urol 148:974–978

Meagher T, Sukmar VP, Collingwodd J et al (2001) Low dose computed tomography in suspected acute colic. Clin Radiol 56:873–876

Memarsadeghi M, Heinz-Peer G, Helbich TH et al (2005) Unenhanced multi-detector row CT in patients suspected of having urinary stone disease: effect of section width on diagnosis. Radiology 235:530–536

Menon M, Resnick MI (2002) Urinary lithiasis: etiology, diagnosis, and medical management. In: Walsh PC, Retik AB, Darracott VE Jr (eds) Campbell's urology. WB Saunders, Philadelphia, pp 3229–3305

Michaels EK, Nakagawa Y, Miura N et al (1994) Racial gender variation in gender frequency of calcium urolithiasis. J Urol 152: 2228–2231

Middleton WD, Dodds WJ, Lawson TL et al (1988) Renal calculi: sensitivity for detection with US. Radiology 167:239–244

Miller OF, Kane CJ (2000) Unenhanced helical computed tomography in the evaluation of acute flank pain. Curr Opin Urol 10:123–129

Mortensen JD, Emmett JL (1954) Nephrocalcinosis: a collective and clinicopathological study. J Urol 71:398–406

Nakada SY, Douglas GH, Attai S et al (2000) Determination of stone composition by noncontrast spiral computed tomography in the clinical setting. Urology 55:816–819

Nawfel RD, Judy PF, Schleipman AR et al (2004) Patient radiation dose at CT urography and conventional urography. Radiology 232:126–132

Niall O, Russell J, MacGregor R et al (1999) A comparison of noncontrast computerized tomography with excretory urography in the assessment of acute flank pain. J Urol 161(2):534–537

Ozdemir H, Demir MK, Temizöz O et al (2008) Phase inversion harmonic imaging improves assessment of renal calculi: a comparison with fundamental gray-scale sonography. J Clin Ultrasound 36(1):16–19

Patel U, Walkden RM, Ghani KR et al (2009) Three-dimensional CT pyelography for planning of percutaneous nephrostolithotomy: accuracy of stone measurement, stone depiction and pelvicalyceal reconstruction. Eur Radiol 19:1280–1288

Pfister SA, Deckaret A, Laschke S et al (2003) Unenhanced helical computed tomography vs intravenous urography in patients with acute flank pain:accuracy and economic impact in a randomized prospective trial. Eur Radiol 13:2513–2520

Platt JF (1992) Duplex Doppler evaluation of native kidney dysfunction. Obstructive and nonobstructive disease. AJR Am J Roentgenol 158:1035–1042

Platt JF (1996) Urinary obstruction. Radiol Clin North Am 34:1113–1129

Platt JF, Rubin JM, Ellis JH (1989a) Distinction between obstructive and non obstructive pyelocaliectasis with Duplex Doppler sonography. AJR Am J Roentgenol 153:997–1000

Platt JF, Rubin JM, Ellis JH et al (1989b) Duplex Doppler US of the kidney: differentiation of obstructive and nonobstructive dilatation. Radiology 171:515–517

Platt JF, Rubin JM, Ellis JH (1993) Acute renal obstruction: evaluation with intrarenal duplex Doppler and conventional US. Radiology 186:685–688

Ramello A, Vitale C, Marangella M (2000) Epidemiology of nephrolithiasis. J Nephrol 13(Suppl 3):S65–S70

Rivers K, Shetty S, Menon M (2000) When and how to evaluate a patient with nephrolithiasis. Urol Clin North Am 27:203–213

Rucker CR, Menias CO, Bhalla S (2004) Mimics of renal colic: alternative diagnoses at unenhanced helical CT. Radiographics 27:S11–S28

Sandhu C, Anson KM, Patel U (2003) Urinary tract stones – part I: role of radiological imaging in diagnosis and treatment planning. Clin Radiol 58:415–421

Saw KC, McAteer JA, Monga AG et al (2000) Helical CT of urinary calculi: effect of stone composition, stone size, and scan collimation. AJR Am J Roentgenol 175:329–332

Scales CD, Curtis LH, Norris R et al (2007) Changing gender prevalence of stone disease. J Urol 177:979–982

Scheffel H, Stolzman P, Frauenfelder T et al (2007) Dual-energy contrast-enhanced computed tomography for the detection of urinary stone disease. Invest Radiol 42:823–829

Schwartz B, Schenkman N, Armenakas N et al (1999) Imaging characteristics of indinavir calculi. J Urol 161:1085–1087

Segal AJ, Spataro RF, Linke CA et al (1978) Diagnosis of nonopaque calculi by computed tomography. Radiology 129:447–450

Segura JW, Preminger GM, Assimos DG et al (1997) Ureteral Stones Clinical Guidelines Panel summary report on the management of ureteral calculi. J Urol 158:1915–1921

Silverman SG, Leyendecker JR, Amis ES Jr (2009) What is the current role of CT urography and MR urography in the evaluation of the urinary tract? Radiology 250:309–323

Smith RC, Rosenfield AT, Choe KA et al (1995) Acute flank pain: comparison of non-contrasted CT and intravenous urography. Radiology 194:789–794

Smith RC, Verga M, Dalrymple N et al (1996) Acute ureteral obstruction: value of secondary signs of helical unenhanced CT. AJR Am J Roentgenol 167(5):1109–1113

Sourtzis S, Thibeau JF, Damry N et al (1999) Radiologic investigation of renal colic: unenhanced helical CT compared with excretory urography. AJR Am J Roentgenol 172(6):1491–1494

Spirnak JP, Resnick MI, Banner MP (1990) Calculus disease of the urinary tract. In: Davidson AJ, Hartman D (eds) Radiology of the kidney and urinary tract. WB Saunders, Philadelphia, pp 53–96

Svedström E, Alanen A, Nurmi M (1990) Radiologic diagnosis of renal colic: the role of plain film, excretory urography and sonography. Eur J Radiol 11(3):180–183

Tack D, Sourtzis S, Dellpierre I et al (2003) Low dose multidetector CT of patients with suspected renal colic. AJR Am J Roentgenol 180:305–311

Taourel P, Thuret R, Hoquet MD et al (2008) Computed tomography in the nontraumatic renal causes of acute flank pain. Semin Ultrasound CT MRI 29:341–352

Tchelepi H, Ralls PW (2009) Color comet-tail artifact: clinical applications. AJR Am J Roentgenol 192:11–18

Teichman JMH (2004) Acute renal colic from ureteral calculus. N Engl J Med 350:684–693

Thomas C, Patschan O, Ketelsen D et al (2009) Dual-energy CT for the characterization of urinary calculi: in vitro and in vivo evaluation of a low-dose scanning protocol. Eur Radiol 19:1553–1559

Townsend BA, Silverman SG, Mortele KJ et al (2009) Current use of computed tomographic urography: survey of the Society of Uroradiology. J Comput Assist Tomogr 33:96–100

Traubici J, Neitlich JD, Smith RC (1999) Distinguishing pelvic phleboliths from distal ureteral stones on routine unenhanced helical CT: is there a radiolucent center? AJR Am J Roentgenol 172:13–17

Tublin ME, Dodd GD 3rd, Verdile VP (1994) Acute renal colic: diagnosis with duplex Doppler US. Radiology 193:697–701

Wrong OM, Feest TG (1976) Nephrocalcinosis. In: Peters DK (ed) Advanced medicine no 12. Pitman Medical, London, pp 394–406